Dynamic Light Scattering Microrheology Reveals Multiscale Viscoelasticity of Polymer Gels and Precious Biological Materials

Supporting Information

Brad A. Krajina, Carolina Tropini, Audrey Zhu, Philip DiGiacomo, Justin L. Sonnenburg, Sarah C. Heilshorn, and Andrew J. Spakowitz*

E-mail: ajspakow@stanford.edu

Methods

Safety statement

No unexpected or unusually high safety hazards were encountered in this work.

Materials

Polyacrylamide gels with varying compositions were prepared by appropriate dilution of a stock solution of 30% acrylamide/bis-acrylamide (37.5:1 acrylamide:bis-acrylamide, Bio-Rad #1610158). Solutions were diluted with MilliQ water. For DLSμR, 100 nm carboxylated polystyrene beads (Polysciences #16688-15) were incorporated in the gel precursor solution to a final concentration of 0.1% w/v. To initiate polymerization, Tetramethylethylenediamine (TEMED) and ammonium persulfate (APS) were added to a final composition of 0.25 % w/v each.

Linear DNA solutions were prepared using the pCMVgluc plasmid (New England Biolabs #N8081S) by restriction digest with HINDIII (New England Biolabs #R3104), followed by phenol chloroform extraction and resuspension in 10 mM Tris-HCl buffer.

Carboxylated polystyrene microspheres were used as as provided by the supplier (Polysciences) or after polyethylene glycol surface functionalization. Polyethylene glycol-functionalized polystyrene microspheres were prepared by EDC/sulfo-NHS ester coupling of carboxylated microspheres to polyethylene gycol diamine ($M_n \sim 2000$ Da, Sigma #753084) as described below in "Preparation of poly(ethylene glycol) (PEG) functionalized tracer particles."

Growth factor reduced Matrigel was used as provided by the supplier (Corning #356230).

DLSμR measurements

DLSμR was performed using a Malvern Zetasizer Nano ZS (633 nm laser) operated in 173° non-invasive backscatter detection mode. For gels, we find that it is essential to isolate the instrument from mechanical vibrations, which we achieve by situating the instrument on a bench-top mechanical vibration isolation system (Minus K Technology #50BM-8). Low-volume measurements are performed using 12 μL quartz cuvettes (Malvern ZEN2112). Raw intensity autocorrelation functions $g^{(2)}(\tau)$ are obtained by modifying the "particle size" SOP and exporting the correlation data from the Zetasizer software. Autocorrelations are collected at a specified measurement position (4.2 mm) for at least 30 minutes.

The Zetasizer Nano ZS is equipped with a translating lens that enables the measurement position within the cuvette to be specified to within 100 μm. For materials with broken ergodicity, the time-averaged scattering intensity at a particular position $\langle I_t \rangle$ is in general not equal to the ensemble averaged scattering intensity $\langle I_e \rangle$ averaged over spatial measurement positions. To correct for broken ergodicity, we determine the ensemble averaged scattering intensity by collecting the time-averaged scattering intensity at 20 different measurement positions in 100 μm increments for 1 minute at each measurement position. The range of measurement positions was selected as that which produces a constant autocorrelation

function for tracer particles diffusing in water at concentrations equal to those used for microrheology. This ensures that the correlation function is not corrupted by cuvette wall flare effects or multiple scattering. This procedure is automated using the SOP player function in the Zetasizer Nano ZS, and populating the SOP playlist with "particle size" measurement SOPs with the desired fixed measurement positions specified. Automatic attenuator selection is used, and the derived photon count rate is used to determine the scattering intensity at each position.

Macrorheology

Oscillatory rheology was performed on polyacrylamide gels and Matrigel using a stress-controlled rheometer (ARG2, TA Instruments) with a 20 mm 1° cone and plate geometry with a geometry gap of 28 μm. Frequency-dependent shear moduli were obtained from frequency sweeps collected at 1% strain. For all materials, strain sweeps were performed from 0.1 to 10% strain at a fixed angular frequency of $\omega = 1$ s^{-1} to confirm that measurements were performed in the linear viscoelastic regime. Sample dehydration was prevented using a water solvent trap. Polyacrylamide gels were allowed to polymerize for 1 hour at the desired temperature prior to conducting measurements. For time-temperature measurements on Matrigel, the liquid was initially cast on the rheometer at 4° C and allowed to equilibrate at each temperature for 30 minutes prior to measurement.

Isolation of mouse intestinal mucus

All animal experiments were performed in accordance with the Stanford Institutional Animal Care and Use Committee. Swiss Webster females between 8-12 weeks of age. Mice were fed were fed an autoclaved standard diet (Purina LabDiet 5K67). To induce colitis, the sample mice were subjected to 5 days of 4% w/v DSS water, followed by 1 day with non-supplemented water. Mice were sacrificed by carbon dioxide asphyxiation followed by cervical dislocation. The intestines were sectioned out and mucus was gently squeezed from the

colon after removing stool and intestinal contents. The mucus was immediately stored in cuvettes and analyzed to minimize evaporation. Each mucus measurement combined 3-5 mice. DLSμR measurements were performed using 1000 nm diameter polyethylene glycol-functionalized polystyrene beads.

Confocal imaging of mouse colon

Distal colon sections were collected and immediately fixed in methacarn solution and processed in paraffin as previously described.[1,2] 4 μm section slices were cut from the paraffin blocks and deparaffinized for immunofluorescence as previously described.[1,2] Mucus was stained with Ulex Europaeus Agglutinin I (UEA-1) and DNA was labeled with 4,6-diamidino-2-phenylindole (DAPI). Images were collected using a Zeiss LSM 880 confocal microscope with the ZEN 2012 software.

Preparation of poly(ethylene glycol) (PEG) functionalized tracer particles

PEG-functionalized polystyrene microspheres were prepared by coupling carboxylated microspheres (Polysciences) to 2000 Da PEG diamine (Sigma #753084) by EDC/sulfo-NHS ester chemistry. Prior to copuling, microspheres were washed three times by centrifuging at $900 \times g$ and resuspending in 50 mM pH 6.0 MES buffer to a final concentration of 1.3% (w/v). ethyl-3-(3-dimethylaminopropyl)carbodiimide hydrochloride (Thermo Fisher # 22980) and sulfo-NHS (Thermo Fisher #24510) were added to the particle suspension to final concentrations of 2 mM and 5 mM, respectively. The suspension was gently rocked for 30 minutes at room temperature. Next, an equal volume of 2 mM PEG diamine buffer solution (100 mM sodium bicarbonate, pH 8.0) was added to the suspension. The mixture was rocked gently for 30 minutes at room temperature. The reaction was quenched by addition of an equal volume of 100 mM glycine, followed by rocking for 30 minutes at room temperature. Finally,

the PEG-functionalized microspheres were washed 10 times by repeatedly centrifuging at $9000 \times g$ for 3 minutes and resuspending in MilliQ water.

Microrheology of polyacrylamide gels

Polyacrylamide gel precursor solutions containing 100 nm carboxylated polystyrene beads were transferred to a 12 μL quartz cuvette immediately after addition of TEMED and APS. The material was allowed to gel for 1 hour. Scattering autocorrelations functions were collected for 1 hour, followed by a sweep over measurements positions in the cuvette to determine $\langle I_e \rangle$.

Cross-over time-scale in polyacrylamide gels

We estimate the time-scale for cross-over from elastic behavior to high-frequency polymer relaxations $\tau_c = \omega_c^{-1}$ by performing independent power-law fits in the frequency range where the shear modulus exhibits plateau modulus behavior and where the modulus exhibits its terminal high-frequency scaling. The cross-over time-scale is estimated based on the frequency at which these two power-law fits intersect, and exhibits a strong dependence on the stiffness of polyacrylamide gels (Supporting Figure 1).

Microrheology of linear DNA solutions

Microrheology measurements on linear DNA were performed using 500 nm carboxylated beads mixed at a final concentration of 0.1% (w/v) by gentle pipetting until the solution was optically homogeneous. The ends of pipette tips were cut to reduce shearing during mixing. DLSμR measurements were performed by collecting autocorrelation functions for 30 minutes at 23° C in a 12 μL quartz cuvette. To confirm independence of the results on bead size, measurements were performed using both 500 nm and 1000 nm diameter beads (Supporting Figure 2).

Microrheology of Matrigel

For DLSμR measurements, growth factor reduced Matrigel basement membrane (Corning #356230) was mixed with PEG-functionalized 500 nm diameter polystyrene beads on ice to a final bead concentration of 0.1% w/v. $12\mu L$ of sample was transferred to a low-volume quartz cuvette that was pre-chilled at 4° C. Samples were allowed to equilibrate at each temperature for 30 minutes, and autocorrelation functions were collected for 30 minutes, followed by a sweep over measurements positions in the cuvette to determine $\langle I_e \rangle$. Measurements were performed in order of increasing temperature. DLSμR measurements conducted at 37° C were compared to macrorheology measurements for validation (Supporting Figure 3).

Optimization of surface chemistry for intestinal mucus measurements

To ensure that the motions of tracer particles within the medium of interest reflect the true shear modulus of the material, it is necessary to incorporate particles whose surface chemistry does not lead to interactions with the material that violate the generalized Einstein-Stokes relation. If macrorheology measurements are available, the appropriate surface chemistry can be determined by comparison between DLSμR and macrorheology. Since macrorheology measurements are impractical for mouse intestinal mucus, we selected the appropriate surface chemistry based on measurements on reconstituted porcine type III stomach mucin (Sigma #M1778) , which is far easier to obtain in sufficient quantities for macrorheology.

We compare DLSμR to macrorheology on porcine mucus (reconstituted to 6% w/v using deionized water) using either carboxylated or PEG-functionalized (PEGylated) 1000 nm diameter polystyrene spheres (Supporting Figure 4). We find that carboxylated particles substantially over-estimate G^* compared to macrorheology. However, the PEGylated particles provide excellent agreement with macrorheology in the frequency range over which the two techniques overlap. Thus, we conclude that the PEGylated particles represent the

appropriate surface chemistry for measurements on mucus, and used these particles for all murine intestinal mucus experiments. In general, we have found that the PEGylated surface chemistry is often preferable for biological materials, including hydrogels formed from extracellular matrices.

Analysis of DLSμR data

Raw intensity autocorrelation functions are analyzed using our custom software written in Python. For ergodic samples, the scattering intensity autocorrelation $g^{(2)}(\tau)$ as a function of the time-lag τ is related to the intermediate scattering function $g^{(1)}(\tau)$ according to,[3]

$$g^{(2)}(\tau) = 1 + (g_0 - 1)|g^{(1)}|^2 \tag{1}$$

where g_0 is the intercept of $g^{(2)}$ at $\tau = 0$.

For non-ergodic materials, the scattering intensity is a superposition of a component due to frozen-in density fluctuations and a component due to dynamic fluctuations, and Eqn. 1 no longer applies.[4] In this case, it is necessary to isolate the component of the scattering intensity that is due to dynamic fluctuations in order to determine the intermediate scattering function, and in turn, the tracer particle mean-squared displacement. This can be accomplished by performing full ensemble averaging of the autocorrelation function over spatial positions. However, due to the time required to collect converged photon statistics in gels (about 30 minutes per measurement position), this is extremely time-consuming and impractical. Alternatively, the intermediate scattering function associated with a particular measurement volume can be extracted by performing a longer time-averaged measurement at the position of interest to extract $\langle I_t \rangle$ and $g^{(2)}$, and determining the ensemble averaged scattering intensity $\langle I_e \rangle$ by performing a series shorter measurements across a range of measurement positions (as described in the previous section). We implement the latter method in this work. Under this method, the intermediate scattering function is extracted from $g^{(2)}$,

$\langle I_t \rangle$, and $\langle I_e \rangle$ according to,[4]

$$g^{(1)}(\tau) = \frac{Y-1}{Y} + \sqrt{(g^{(2)}(\tau) - g_0)}/Y \tag{2}$$

where $Y = \langle I_e \rangle / \langle I_t \rangle$.

The tracer particle mean-squared displacement $\langle \Delta r^2(\tau)$ is in turn related to the intermediate scattering function by

$$g^{(1)}(\tau) = \exp(\frac{-q^2 \Delta r^2(\tau)}{6}) \tag{3}$$

where q is the scattering vector, which is related to the scattering angle θ, the index of refraction of the medium n and the wavelength of the laser λ according to $q = \frac{4\pi n \sin(\theta/2)}{\lambda}$.

Finally, the unilateral Fourier transform of the particle mean-squared displacement $\langle \Delta r^2(\omega) \rangle$ for tracer particles with radius a can be used to extract the frequency-dependent shear modulus $G^*(\omega)$ using the generalized Stokes-Einstein relation,[5]

$$G^*(\omega) = \frac{k_B T}{\pi a i \omega \langle \Delta r^2(\omega) \rangle} \tag{4}$$

To avoid truncation errors associated with the Fourier transform, we conduct a local power-law analysis developed by Mason and co-workers by performing a sliding window linear regression with Gaussian weights on $\langle \Delta r^2(\tau) \rangle$ in logarithmic space and time.[5]

Reliable determination of the intensity autocorrelation intercept g_0 is essential to the analysis described above, and is particularly important for the high-frequency data. Since the photon correlator provides values of $g^{(2)}$ only down to time lags of 0.5 μs, it is necessary to estimate the intercept by extrapolation. We estimate the intercept by fitting $g^{(2)}(\tau)$ to a functional form at early time delays and using the intercept of the fitted function for the value of g_0. We find that for all materials considered in this work, an excellent fit can be

obtained by fitting $g^{(2)}$ to either a stretched exponential,

$$g^{(2)}(\tau) = g_0 \exp(-(\frac{\tau}{\tau_0})^{\beta}) \tag{5}$$

or a function of the form,

$$g^{(2)}(\tau) = g_0 \exp(-\lambda(1 - \exp(-(\frac{\tau}{\tau_0})^{\beta})) \tag{6}$$

where τ_0, g_0, λ, and β are fitting parameters. We find that the latter form is most well-suited for permanently cross-linked gels, whereas the stretched exponential is superior for other materials in this work.

It is necessary to appropriately select the fitting window for intercept estimation. Fitting windows that are too small result in over-fitting with respect to noise in the early time portion of the data. Fitting windows that are too large result in poor intercept estimation due to deviations of the fit from the data. To achieve the appropriate balance between fit error and over-fitting, we perform leave-one-out cross-validation on the fit and select the fitting window that provides the lowest cross-validation error.

Scaling analysis of Zimm relaxations in polyacrylamide gels

Our scaling analysis for prediction of the high-frequency Zimm relaxation of branched polymer fractals is analogous to the scaling analysis for Rouse fractal clusters at the percolation point.[6] Percolation theory predicts that at the gel point, a percolating network of branched fractal clusters is formed in which each polymer sub-section within the fractal cluster exists at the critical overlap concentration with surrounding fractal chains of similar size. We assume that the gel formed above the gel point consists of a network of effective elastic chains whose internal structure mirrors the space-filling branched fractal structure of percolating clusters formed during gelation. Such a structure may be expected to arise if the small length-scale structures present in the fractal clusters are quenched into the gel during the

formation of a mature percolating network. If the elastic network consists of effective elastic chains with size equal to the gel correlation length ξ, then each effective elastic chain will contribute k_BT to the thermal energy stored in the gel, in accordance with equipartition of energy. Hence, the plateau modulus G_0 will scale with the size of effective elastic chains according to:

$$G_0 \sim \frac{k_BT}{\xi^3} \tag{7}$$

Suppose each elastic chain is a branched fractal consisting of self-similar polymer "blobs" that are also space-filling and exhibit relaxation on time-scales τ_p, where p is a "blob" index. Then after a step strain is applied, each unrelaxed fractal "blob" will contribute k_bT to the to the stored energy. Thus, the stress relaxation function $G(\tau)$ after a time τ_p will scale with the size of the fractal "blobs" ξ_p that relax on time-scale τ_p according to:

$$G(\tau_p) \sim \frac{k_BT}{\xi_p^3} \tag{8}$$

At long times, all "blobs" within the fractal effective elastic chains that form the percolating network will have fully relaxed, other than the elastic modes contributed by the effective elastic chains themselves, and the stress relaxation function will converge to the plateau shear modulus.

The characteristic relaxation time of a "blob" with size ξ_p scales according to the time required for the "blob" to diffuse a distance of its own size. If each "blob" exhibits non-draining (Zimm) hydrodynamic interactions, the characteristic time-scale for relaxation scales with the "blob" size according to:

$$\tau_p \sim \xi_p^3 \tag{9}$$

Note that although this relaxation behavior is most well-known for linear gaussian chains, it has been generalized for branched polymers of arbitrary fractal dimension in the strong hydrodynamic coupling limit .[7] Equivalently, each "blob" of size ξ_p will relax at a character-

istic frequency $\omega_p \sim \tau_p^{-1}$, and the frequency-dependent shear modulus $G(\omega)$ will scale with frequency according to:

$$G(\omega) \sim \omega \tag{10}$$

This scaling analysis produces the same scaling behavior that is predicted by percolation theory for the relaxation spectrum of fractal clusters at the critical gel point when strong hydrodynamic interactions are present.[8] This analysis also agrees with the high-frequency scaling limit predicted by detailed derivation of the viscoelasticity for dilute solutions of branched polymer fractals of fractal dimension $D_f = 3$ with strong hydrodynamic interactions .[7] Note that the fractal dimension $D_f = 3$ is compatible with our assumption that the effective elastic chain is space-filling fractal.

Theoretical predictions for a wormlike chain (WLC)

Theoretical estimation of the shear modulus of a solution of wormlike chains was performed as described in detail in below. Monte Carlo simulations of a WLC were performed using our previously described coarse-grained simulation procedure.[9,10]

The full analytical solution for G^* of a WLC across all frequencies in semiilute solutions not available. However, the low- and high-frequency scaling behaviors of a sufficiently long wormlike chain are well-known. At high-frequencies, the scaling behavior of G^* for a solution of wormlike chains tends to,[11]

$$G^* = \frac{2^{3/4}}{15}\rho(k_B T)^{1/4} l_p^{5/4} (i\omega\xi_\perp)^{3/4} \tag{11}$$

where symbols are defined in the main text. In the absence of hydrodynamic interactions, for a wormlike chain with a contour length L much greater than its persistence length l_p, the low-frequency behavior will tend to a Rouse polymer. The full-frequency dependence of

a solution of Rouse polymers with a polymer concentration per unit volume c is given by,[12]

$$G' = ck_BT \sum_{p=1}^{\infty} \frac{(\omega\tau_p)^2}{1+(\omega\tau_p)^2}$$
$$G'' = ck_BT \sum_{p=1}^{\infty} \frac{\omega\tau_p}{1+(\omega\tau_p)^2}$$

where τ_p is the relaxation time of the p^{th} normal mode, i.e.

$$\begin{aligned}\tau_p &= \tau_R p^{-2} \\ &= \frac{p^{-2} 2 l_p \xi_R L^2}{3\pi^2 k_B T}\end{aligned}$$

The full frequency-dependence of a solution of wormlike chains must capture these limits at low- and high-frequencies, and interpolate between them at intermediate frequencies. Our previous simulation work on the dynamics of long wormlike chains ($L = 10l_p$) demonstrates that the transition of the stress correlation from the high-frequency WLC behavior to Rouse scaling behavior is rather abrupt.[9] This suggests that the simple interpolation scheme that we implement here and describe below provides a reasonable approximation to the full analytical solution.

We treat the Rouse friction coefficient per unit length ξ_R and the transverse friction coefficient $\xi_\perp$ as the only free fitting parameters in our model. For a given pair of friction coefficients, we estimate the full value of G^* as follows. Let G^*_{WLC} be the high-frequency scaling limit of a WLC and G^*_R be the shear modulus of a Rouse polymer. Let ω^* be the frequency at which $|G^*_{WLC}| = |G^*_R|$. We define $|G^*|$ as the piece-wise function (top plot of Supporting Figure 5),

$$|G^*| = \begin{cases} |G^*_{WLC}| & \omega > \omega^* \\ |G^*_R| & \omega \leq \omega^* \end{cases}$$

We determine the real and imaginary components of G^* (bottom plot of Supporting Figure 5) by noting that $|G^*(\omega)|$ is equivalent to the Laplace-space representation of the shear modulus $\tilde{G}(s)$. Moreover, the Fourier-space representation of the shear modulus $G^*(\omega)$ is related to $\tilde{G}(s)$ by analytic continuation of $\tilde{G}(s)$ onto the imaginary axis in the complex plane, i.e. $G^*(\omega) = \tilde{G}(i\omega)$. We perform this continuation into the complex plane numerically by performing a rolling window linear regression in log-log space of $|G^*(\omega)|$. This is equivalent to locally representing the shear modulus by a power-law of the form $|G^*(\omega)| = b\omega^\alpha$, where α is the slope of the local linear fit in log-log space. The real and imaginary components of G^* are in turn given by

$$G'(\omega) = |G^*(\omega)| \cos(\alpha\pi/2)$$
$$G''(\omega) = |G^*(\omega)| \sin(\alpha\pi/2)$$

We determine $G^*(\omega)$ based on the values of ξ_R and $\xi_\perp$ that provide the best fit between the theoretical prediction and the experimental measurements.

References

(1) Earle, K. A.; Billings, G.; Sigal, M.; Lichtman, J. S.; Hansson, G. C.; Elias, J. E.; Amieva, M. R.; Huang, K. C.; Sonnenburg, J. L. Quantitative Imaging of Gut Microbiota Spatial Organization. *Cell Host & Microbe* **2015**, *18*, 478–488, DOI: 10.1016/j.chom.2015.09.002.

(2) Johansson, M. E. V.; Hansson, G. C. In *Mucins: Methods and Protocols*;

McGuckin, M. A., Thornton, D. J., Eds.; Humana Press: Totowa, NJ, 2012; pp 229–235, DOI: 10.1007/978-1-61779-513-8_13.

(3) Berne, B. J.; Pecora, R. *Dynamic Light Scattering: With Applications to Chemistry, Biology, and Physics*; Wiley: New York, 2003.

(4) Pusey, P. N. Dynamic light scattering by non-ergodic media. *Physica A* **1989**, *157*, 705–741, DOI: 10.1002/masy.19940790104.

(5) Mason, T. G.; Ganesan, K.; van Zanten, J.; Wirtz, D.; Kuo, S. Particle Tracking Microrheology of Complex Fluids. *Physical Review Letters* **1997**, *79*, 3282–3285, DOI: 10.1103/PhysRevLett.79.3282.

(6) Rubinstein, M.; Colby, R. *Polymer Physics*; Oxford University Press: New York, 2003.

(7) Cates, M. E. Brownian dynamics of self-similar macromolecules. *Journal de Physique* **1985**, *46*, 1059–1077, DOI: 10.1051/jphys:019850046070105900.

(8) Martin, J. E.; Adolf, D.; Wilcoxon, J. P. Viscoelasticity of near-critical gels. *Physical Review Letters* **1988**, *61*, 2620–2623, DOI: 10.1103/PhysRevLett.61.2620.

(9) Koslover, E. F.; Spakowitz, A. J. Multiscale dynamics of semiflexible polymers from a universal coarse-graining procedure. *Physical Review E* **2014**, *90*, 013304, DOI: 10.1103/PhysRevE.90.013304.

(10) Koslover, E. F.; Spakowitz, A. J. Discretizing elastic chains for coarse-grained polymer models. *Soft Matter* **2013**, *9*, 7016–7027, DOI: 10.1021/ma302056v.

(11) Morse, D. C. Viscoelasticity of Concentrated Isotropic Solutions of Semiflexible Polymers. 1. Model and Stress Tensor. *Macromolecules* **1998**, *31*, 7030–7043, DOI: 10.1021/ma9803032.

(12) Doi, M.; Edwards, S. *The Theory of Polymer Dynamics*; Clarendon Press: Oxford, 1988.

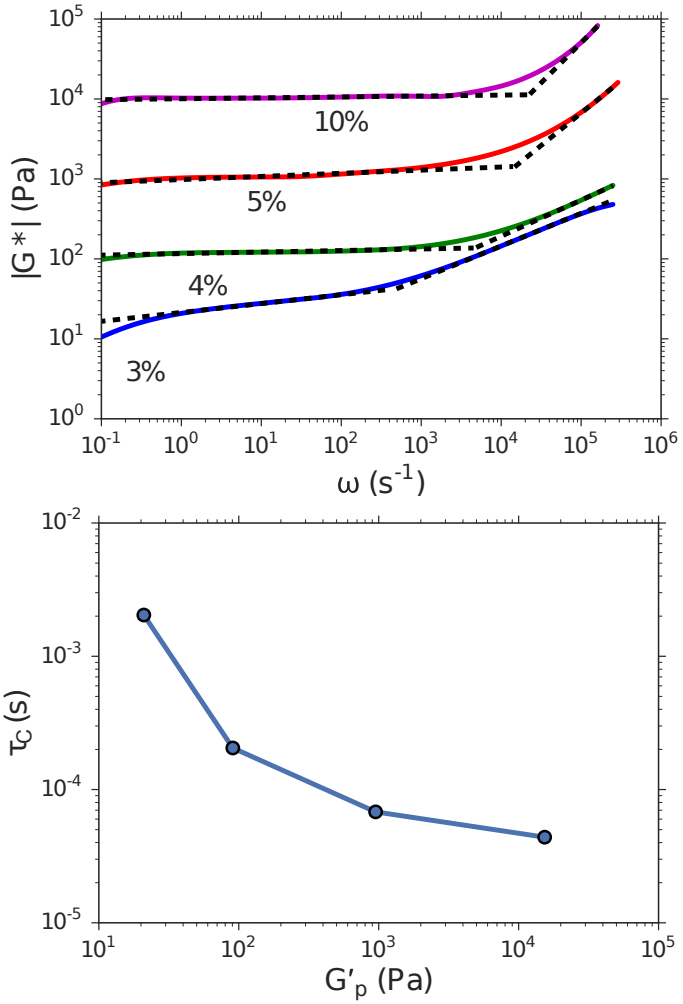

Supporting Figure 1: Cross-over time-scale for the transition from plateau elastic behavior to high-frequency polymer relaxations in polyacrylamide gels. *Top*: Power-law fitting to $|G^*|$ as a function of frequency ω. Dashed lines indicate power-law fits in the plateau modulus regime and the high-frequency regime. Solid lines indicate experimental data for polyacrylamide gels with the indicated acrylamide concentrations. *Bottom*: Time-scale for cross-over to the high-frequency scaling regime as a function of the plateau storage modulus $G'_p = G'(\omega = 10\text{rad/s})$ for the gels with varying composition in the top plot.

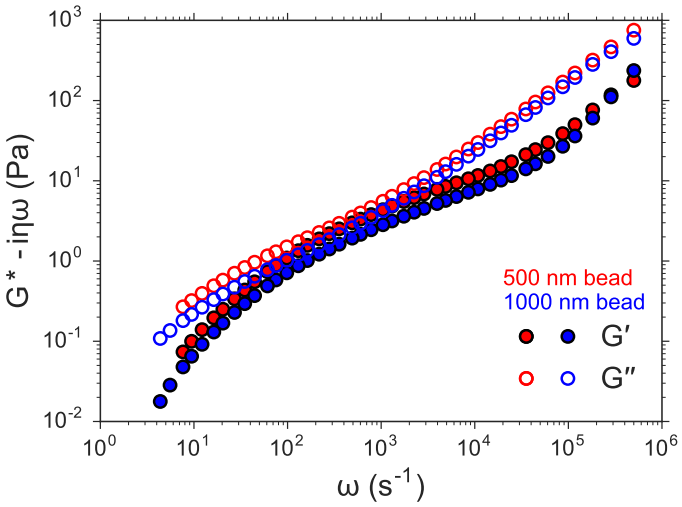

Supporting Figure 2: DLSμR measurements on semidilute DNA solutions are weakly dependent on particle size for probe particles with diameters of at least 500 nm. The dependence of G^* on angular frequency ω for 1.0 mg/mL solutions of linear DNA (5.8 kilobases) was compared for 500 nm and 1000 nm diameter tracer particles (red and blue, respectively), revealing a small dependence on the size of the tracer particles.

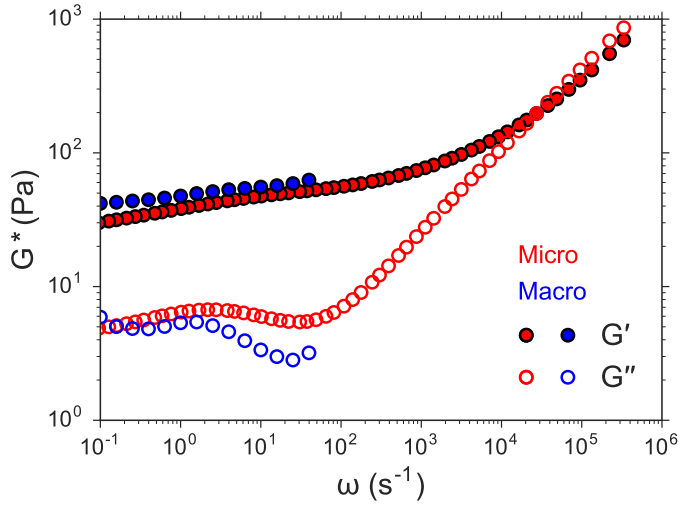

Supporting Figure 3: DLSμR on Matrigel recapitulates macrorheology. Comparison of DLSμR (red) and macrorheology (blue) measurements of the dependence of the shear modulus G^* on angular frequency ω at 37° C

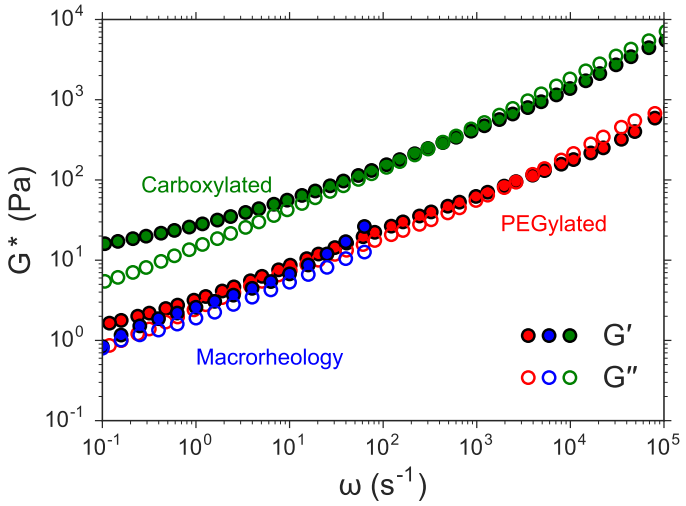

Supporting Figure 4: Effect of tracer particle surface chemistry on DLSμR of reconstituted porcine stomach mucus.

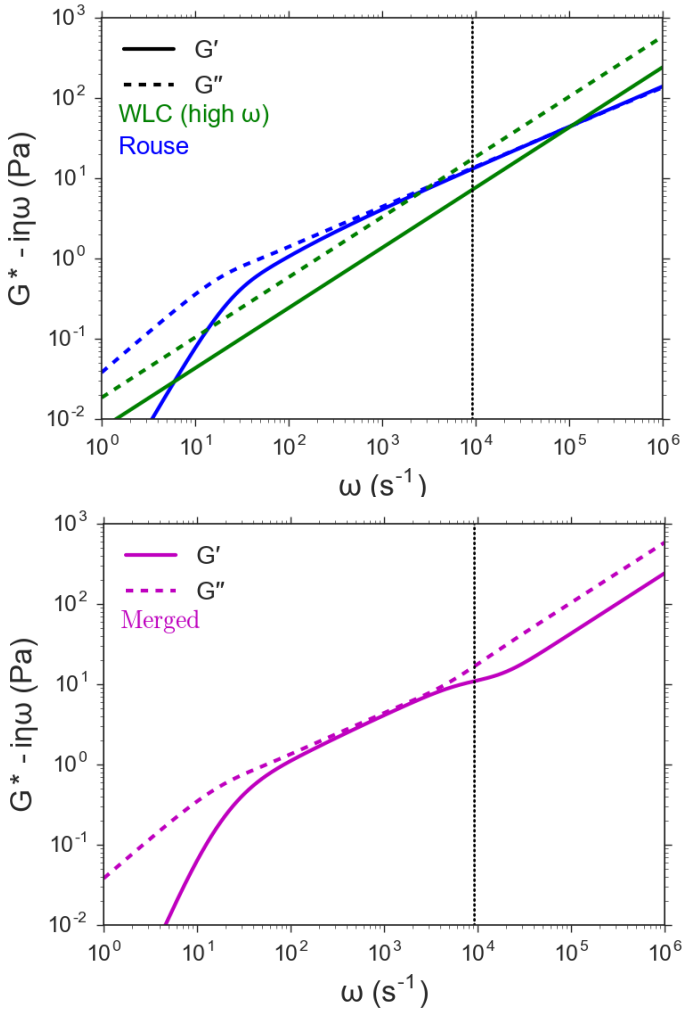

Supporting Figure 5: Theoretical prediction for the frequency-dependence of G^* for a WLC. *Top*: Theoretical predictions for a Rouse polymer (blue) and the high-frequency behavior of a WLC (green). The vertical dotted line indicates the frequency ω^* at which $|G^*|$ is equal for these two models. *Bottom* Estimation of the full frequency dependence of G^* of a WLC obtained by the matching procedure described in the text.